







Dynamics of all-optically switched magnetic domains in Co/Gd heterostructures with Dzyaloshinskii-Moriya interaction

Anni Cao ^{1,2}, Yuri L. W. van Hees ¹, Reinoud Lavrijsen ¹, Weisheng Zhao ^{2,*} and Bert Koopmans ^{1,†}

¹*Department of Applied Physics, Institute for Photonic Integration, Eindhoven University of Technology, PO Box 513, 5600 MB Eindhoven, The Netherlands*

²*Fert Beijing Institute, Beijing Advanced Innovation Center for Big Data and Brain Computing, School of Microelectronics, Beihang University, Beijing 100191, China*

 (Received 25 May 2020; revised 8 July 2020; accepted 17 August 2020; published 9 September 2020)

Given the development of hybrid spintronic-photonic devices and optical manipulation of chiral magnetic textures, a combined interest in single-pulse all-optical switching (AOS) of magnetization and current-induced domain wall motion in synthetic ferrimagnetic structures with strong Dzyaloshinskii-Moriya Interaction (DMI) is emerging. In this work, we explore the role of the DMI on the AOS process as well as the stability of optically written micromagnetic domains using specially engineered Co/Gd-based multilayer structures. Quantitative insight is obtained by measuring the interesting dynamics in moon-shaped structures written by two successive laser pulses. The stability of domains resulting from an interplay between the dipolar interaction and domain-wall energy are compared to simple analytical models and micromagnetic simulations. A shortening process occurring at ns time scale is confirmed by our computational results, and a stabilizing role of DMI on microscopic AOS-written domains is experimentally demonstrated.

DOI: [10.1103/PhysRevB.102.104412](https://doi.org/10.1103/PhysRevB.102.104412)

I. INTRODUCTION

After the observation of helicity-dependent switching in ferrimagnetic GdFeCo alloys [1,2] in 2007, all-optical switching (AOS) attracted a growing amount of interest as an ultrafast and energy-saving writing process for spintronic devices. This helicity-dependent switching description has been found appropriate for various magnetic materials [3–6], however, for most materials with a disadvantage that hundreds of pulses are required for the switch [6]. At the same time, based on another mechanism, purely thermal toggle switching was demonstrated in rare-earth-transition-metal alloys, governed by the large difference in demagnetization rates and antiferromagnetic exchange [7–10]. Later, it was predicted and proved that synthetic-ferrimagnetic systems can also be thermally toggle-switched by a single laser pulse [11–14]. More specifically this was experimentally demonstrated in Pt/Co/Gd systems. Meanwhile, in the field of spintronics, an antisymmetric exchange interaction, the Dzyaloshinskii-Moriya Interaction (DMI), has been intensively investigated. It appears in inversion asymmetric structures and participates in the competition with exchange interaction and dipolar interaction to influence chiral spin textures. Considering the structural-asymmetry in synthetic-ferrimagnetic multilayers, the built-in DMI could be expected to play a major role in the switching process, as well as in the stability of the toggle-pulse-switched domains, but this has not been explored to date. Recently, a combination of racetrack memory [15]

and AOS has been experimentally demonstrated in an on-the-fly demonstration of optically writing information into a magnetic racetrack [16]. In the latter work, current-induced domain wall motion (driven by the spin Hall effect) was ascribed to a strong spin-orbit torque in combination with DMI. For synthetic ferrimagnetic systems near the angular momentum compensation point, this scenario is known to enable high domain wall velocities [16]. Looking into the role of DMI on the AOS process is not only significant for improving the storage density and stability of such optically written racetrack devices, but also for AOS-related magnetic random-access memory.

In this paper, we employed synthetic-ferrimagnetic Pt/Co/Gd stacks for studying the role of DMI on AOS, and particularly the stability of AOS written domains. The strong antiferromagnetic coupling at the Co/Gd interface [16] and the large contrast in demagnetization times between Co and Gd [17,18] ensure the optical-switching of our samples, in a scenario that recently was explained in more detail [19,20]. To manipulate the strength of DMI through structural (a)symmetry, structures with a single ferrimagnetic interface (Co/Gd) and double ferrimagnetic interface (Co/Gd/Co) are proposed. The resulting DMI is measured by asymmetric domain wall motion, and the corresponding threshold fluence for AOS is determined by recording the written domain as a function of laser pulse energy. In order to quantify the role of the DMI on the stability of optically written magnetic domains we introduce a two-pulse approach. Two successive laser pulses were produced to write elongated moon-shaped magnetic domains in our synthetic-ferrimagnetic thin films. We emphasize that the AOS process avoids the use of magnetic fields during the domain formation, whereby results are not

*Corresponding author: weisheng.zhao@buaa.edu.cn

†Corresponding author: b.koopmans@tue.nl

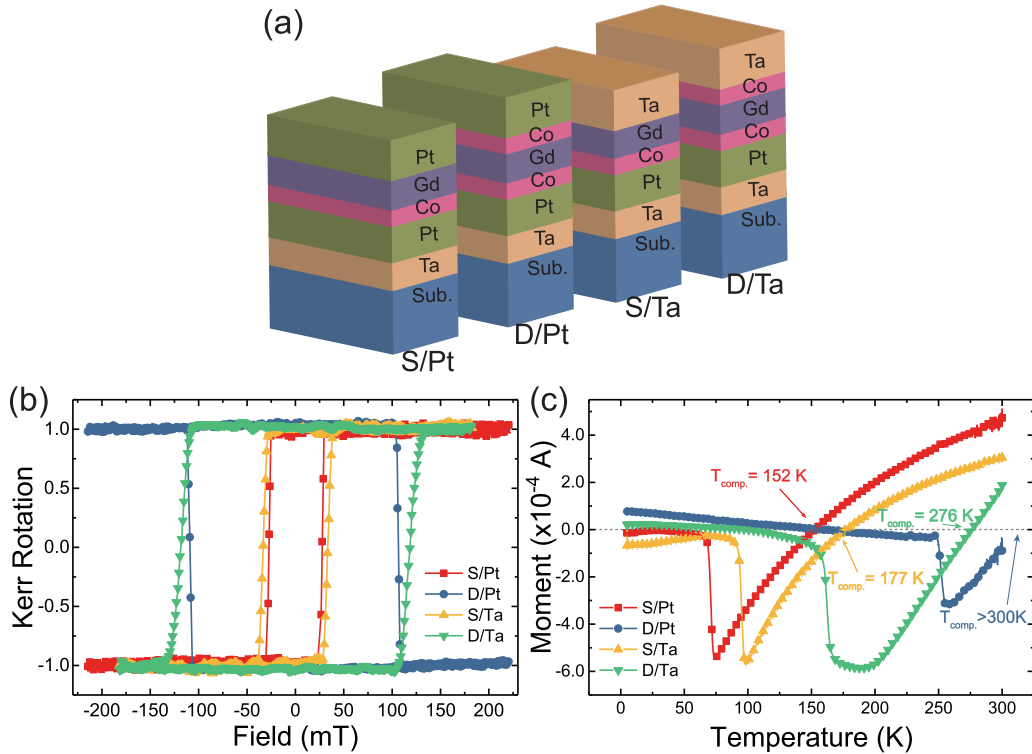


FIG. 1. (a) Samples' structures and (b) normalized hysteresis loops with perpendicular magnetic field for each structure grown on Si/SiO₂. (c) Magnetic moment per unit area as a function of the temperature, with T_{comp} corresponding to the zero-moment marked besides each curve.

affected by field driven domain-wall motion. A simple model including the competition between dipolar interaction and domain-wall energy is proposed, which describes the domain shrinkage at the sharp ends and expansion at their waist. Both the micromagnetic simulation and experimental observations exhibit obvious shrinkage and negligible expansion. Finally, we experimentally demonstrate that DMI is helpful to stabilize the AOS-written small-size domain stripes, in agreement with our model.

II. SAMPLE PREPARATION

To distinguish the strength of DMI through structural asymmetry, we grow samples [see Fig. 1(a)] with single and double Co layers by magnetron sputtering and marked them as **S/Pt**: Ta (4 nm)/Pt (4 nm)/Co (1 nm)/Gd (3 nm)/Pt (4 nm) and **D/Pt**: Ta (4 nm)/Pt (4 nm)/Co (1 nm)/Gd (3 nm)//Co (1 nm)/Pt (4 nm), where S and D refer to single and double. Since time-dependent intermixing (particularly at the Gd/Pt interface) over time scales of days to weeks were observed in a similar structure, we also prepared another pair of structures with different capping layers, **S/Ta** and **D/Ta**, as reference. All of the structures are deposited on two types of substrates, Si:B and silicon with a 100-nm thermal silicon oxide layer (Si/SiO₂). The base pressure of our ultrahigh vacuum deposition system is around 2×10^{-9} mbar. The (111) texture of the bottom Pt was ensured by a Ta seed layer [21], which promotes perpendicular magnetic anisotropy (PMA) induced by the lower Pt/Co interfaces. The PMA is confirmed by polar magneto-optic Kerr effect, as seen in Fig. 1(b).

III. CHARACTERIZATION OF COMPENSATION TEMPERATURE

The Curie temperature of bulk Co is 1403 K while the Curie temperature of bulk Gd (289 K) lies below room temperature (298 K). Considering that the Curie temperature for nanometer-thin films is even lower, the Gd layer will be paramagnetic at room temperature. However, due to the strong antiferromagnetic exchange interaction at the Co/Gd interface, a layer of roughly 1–2 atomic layers will be magnetized oppositely to Co at room temperature. This process is possibly enhanced by thermodynamically driven interdiffusion [22] between Co and Gd, which is expected to be of particular relevance for the top Gd/Co interface in the double-layer structures, leading to a composition at the interface close to a Gd₄₀Co₆₀ alloy [23,24]. The compensation temperature (T_{comp}) is defined as the temperature for which the total magnetic moment of the whole structure vanishes. As a rule of thumb, the higher T_{comp} , the more Gd is inversely magnetized at the Co/Gd interface at room temperature.

We measured the magnetic moment of our samples using the vibrating sample magnetometer (VSM) mode of a superconducting quantum interference device to evaluate the magnetic moment of our stacks as a function of temperature, and, more specifically, T_{comp} , from which we can extract the amount of magnetized Gd at the synthetic-ferrimagnetic Co/Gd interfaces [13]. For each sample, we applied +6 T external field to saturate the film at the start, then turn off the field, and measure the perpendicular component of the magnetic moment at different temperatures. The magnetic moments per unit surface area versus temperature are shown

in Fig. 1(c). While the temperature decreases, the magnetization of the Gd layer increases, and below $T_{\text{comp.}}$, the Gd, instead of the Co layer, starts to dominate the total moment. Upon further decrease of the temperature, the total magnetic moment will rapidly increase (in the direction of the Gd moment), whereby the (in-plane) shape anisotropy will overcome the (perpendicular) interfacial anisotropy, and starts to be dominant. As a result, the easy axis will rotate from out-of-plane to in-plane, as seen in the measurements by a sharp collapse of the magnetic moment for lower temperature [indicated by pointers in Fig. 1(c)]. More details about measuring $T_{\text{comp.}}$ with a bias field and the corresponding temperature-dependent magnetic moments are given in Supplemental Material part I [25].

For a proper interpretation, it is of relevance to note that for structures with two Co layers and a double Co/Gd interface, one would ideally expect both a doubling of the Co moment, as well as the Gd moment. Thus, based on the assumption that the top (Gd/Co) and bottom (Co/Gd) interface are their exact mirror image, one would expect that the $T_{\text{comp.}}$ of double Co/Gd interface structures will be comparable with $T_{\text{comp.}}$ of the single (Co/Gd) interface group. However, as seen in Fig. 1(c), **S/Ta** shows a lower $T_{\text{comp.}}$ (177 K) and a higher room-temperature moment compared with **D/Ta**, which means that the top and bottom interfaces are not identical. More specifically, the higher $T_{\text{comp.}}$ of **D/Ta** would be consistent with a larger induced Gd moment at the top interface. This finding agrees with work by Hufnagel *et al.*, who reported that compared with the case when Co is deposited on Gd, less rapid intermixing is observed when Gd is deposited on Co [22]. The same trend is observed for the samples capped with Pt, albeit they display a higher $T_{\text{comp.}}$ compared to their Ta counterparts, and the difference between **S** and **D** structure is larger. For structures with a single Co layer, the sample capped with Pt (**S/Pt**) exhibits less intermixed Gd compared with **S/Ta**, which might be caused by the intermixing between Gd and the Pt capping layer. Furthermore, note that we did not observe $T_{\text{comp.}}$ below room-temperature for **D/Pt** in Fig. 1(c). However, the inverse Kerr signal, shown in Fig. 1(b), indicates an inverse total moment of the whole structure, which means the Gd moment is larger than the Co moment in **D/Pt**. Therefore, we deduce that **D/Pt** has a $T_{\text{comp.}}$ above room-temperature indeed.

IV. CHARACTERIZATION OF DMI

We quantified the strength of DMI in our samples employing a magneto-optical Kerr microscope to observe asymmetric domain wall (DW) movement in the creep regime with an in-plane field H_x and a perpendicular field H_z . The dependence of DW velocities on the in-plane field is found to display a minimum occurring at a nonzero value of H_x , which we use as an indication of the strength of DMI and mark it as H_{DMI} [26]. A typical result of asymmetrical DW motion in the presence of an in-plane field H_x is shown in Fig. 2(a). The applied $\mu_0 H_z$ is around tens of milli-tesla, and the in-plane field $\mu_0 H_x$ is in the range of ± 350 mT. Due to strong pinning and $T_{\text{comp.}}$ being close to room-temperature, we failed to observe DW motion in sample **D/Pt**. The other three samples displayed a very pronounced asymmetry in the

DW velocity which indicates a sizable DMI. We employed a procedure using an empirical function (see Supplemental Material part II [25]) by which we obtained the values of the effective DMI field H_{DMI} , as shown in Figs. 2(b)–2(d). In a ferromagnetic system, the DMI energy can be extracted by $|D| = \mu_0 M_S |H_{\text{DMI}}| \sqrt{A/K_{\text{eff}}}$ [27], where M_S is the saturation magnetization, A the exchange stiffness, and the K_{eff} effective anisotropy. As we mentioned above, in a Co/Gd system, there is a very thin layer of Gd antiferromagnetically coupled with Co at the Co/Gd interface. It has been reported that the thickness of the antiferromagnetic Gd layer is about 0.5 nm. Although extracting a quantitative value of the DMI parameter D is far from trivial for this system, we performed a simplified analysis to derive a rough estimate. By assuming the thickness of the ferromagnetic layer $t = 1.5$ nm for a single Co structure (**S/Pt** and **S/Ta**) and $t = 3.0$ nm for a double Co structure (**D/Pt** and **D/Ta**), M_S and K_{eff} (averaged over Co and Gd per unit volume) can be calculated based on the VSM data. Taking $A = 16$ pJ/m from literature [28], we estimate $|D| \approx 0.09 \pm 0.01$, 0.24 ± 0.01 , and 0.37 ± 0.01 mJ/m² for **D/Ta**, **S/Ta**, and **S/Pt**, respectively. We do notice that the characterization of DMI by the minimum DW velocity in the creep mode has been intensively debated. Nevertheless, employing the same measurement and a model including the most important contributions to the domain-wall energy, Hartmann *et al.* have reported a $H_{\text{DMI}} \sim 220$ mT in Pt/Co/Gd structure [26], which is close to our result of **S/Pt** as shown in Fig. 2(b). This correspondence may indicate that for our Co/Gd structures creep data provides a reasonable and trustworthy value of the DMI field. However, independent of such a quantitative comparison, the strong asymmetries we measured in the DW velocities are a clear indication of a significant DMI for all samples, and a reduced DMI of the double structure as compared to the single one shown in Figs. 2(c) and 2(d). This is consistent with our expectation that the double-Co-layer structure should be more symmetric, i.e., have a smaller H_{DMI} , because of the inversion symmetry of the Co/Gd and Gd/Co interface. The observation that **D/Ta** still has a finite H_{DMI} , hints again at the nonequivalence of the bottom and top interface, as could be explained by growth-induced differences. We stress that our estimate of $|D|$ is just a rough estimate for several reasons, including but not limited to the uncertainty of t and A . Hereon, we leave the exact value of $|D|$ in our Co/Gd system as an open question for further research.

V. CHARACTERIZATION OF THRESHOLD FLUENCE

We carried out all-optical switching experiments on these synthetic-ferrimagnetic multilayers. All samples were first saturated with an external field and then excited by single laser pulses without applying a magnetic field. Each structure was exposed to linearly polarized laser pulses with 700-nm central wavelength, ~ 100 -fs duration, and a pulse energy up to 1 μ J, focused on typically a spot size of ~ 50 - μ m diameter. The all-optically written domains were imaged after mounting the samples in a Kerr microscope. In this section, we will discuss experiments aimed at exploring the AOS efficiency of the various samples. In the following sections we will report

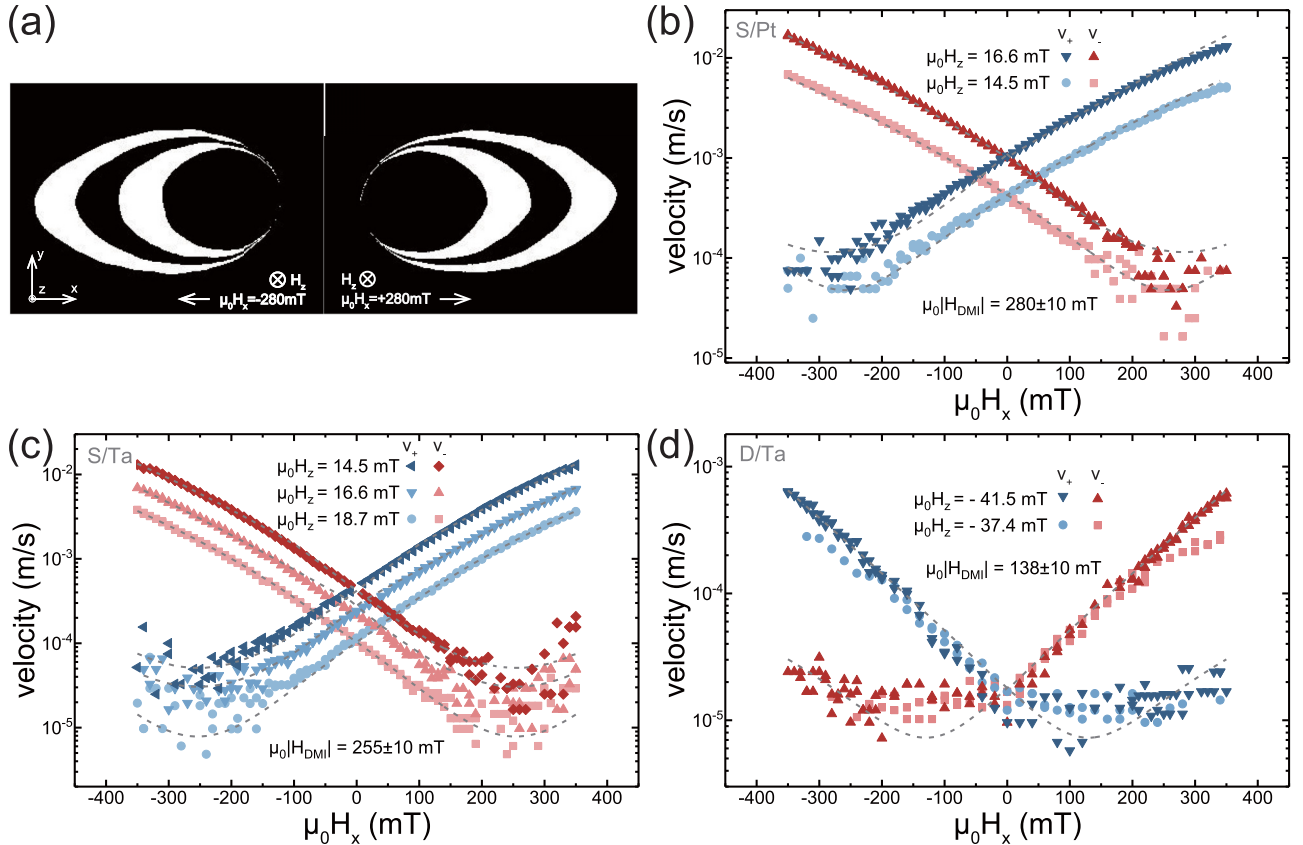


FIG. 2. (a) DW expansion of S/Ta driven by out-of-plane magnetic field $\mu_0 |H_z| = 16.6 \text{ mT}$ with in-plane field $\mu_0 |H_x| = 280 \text{ mT}$. DW velocities of structure S/Pt, S/Ta and D/Ta are shown in (b)–(d) respectively, with $\mu_0 |H_x|$ varying from -350 to 350 mT and corresponding $\mu_0 H_z$ as well as the fitted $\mu_0 |H_{\text{DMI}}|$ (corresponding to the gray dashed lines) are indicated. v_+ (blue symbols) present the domain's velocity along the $+x$ axis, v_- (red symbols) present the domain's velocity along the x axis.

on experimental investigations aimed at understanding the stability of small, optically written micromagnetic domains, after first having provided some physical insight by introducing some simple models.

As outlined above, we start by exploring the AOS efficiency. A threshold fluence F_0 is defined as the threshold pulse energy P_0 divided by the laser spot area A_0 (defined at $1/e$ intensity). Considering the thermal switching mechanism, demagnetization of the magnetic layer is a precondition for magnetization switching. We varied the pulse energy by a neutral density filter wheel and wrote circular domains by single laser pulses, shown in Fig. 3(a). It can be seen that above the threshold energy P_0 , the domain area exhibits a positive correlation with pulse energy. The areas of domains written on the four samples are plotted in Fig. 3(b) as a function of pulse energy. Supposing the energy of the laser pulse shows a Gaussian spatial profile, in the case of an elliptical laser spot, the relation between the domain area and the pulse energy has been derived to be [29]

$$A = 2\pi r\sigma^2 \ln\left(\frac{P}{P_0}\right) = A_0 \ln\left(\frac{P}{A_0 F_0}\right), \quad (1)$$

where σ is the length of the short axis for the elliptical Gaussian spot and r the ratio between the long and short axis. r and σ were determined from the Kerr images, after which A_0 and F_0 can be fitted using Eq. (1). The fitted F_0 of the four structures grown on Si/SiO₂ are smaller than F_0 for structures with Si:B substrate, due to more efficient optical absorption. More details are discussed in Supplemental Material part III [25]. We found that the **S** structure exhibits lower threshold energy P_0 and threshold fluence F_0 than the **D** structure, which speculatively could be explained by a difference in intermixing at the interfaces [19], and/or DMI strength of different structures.

VI. THEORETICAL ANALYSIS OF DOMAINS SHAPE-CHANGE

To understand the stability of small domains after AOS, we will distinguish two types of domains, as can be simply produced by one or two laser pulses. (i) Circular bubbles are written by AOS and using a single pulse, such as shown in Fig. 3(a). Note that these domains are expected to form

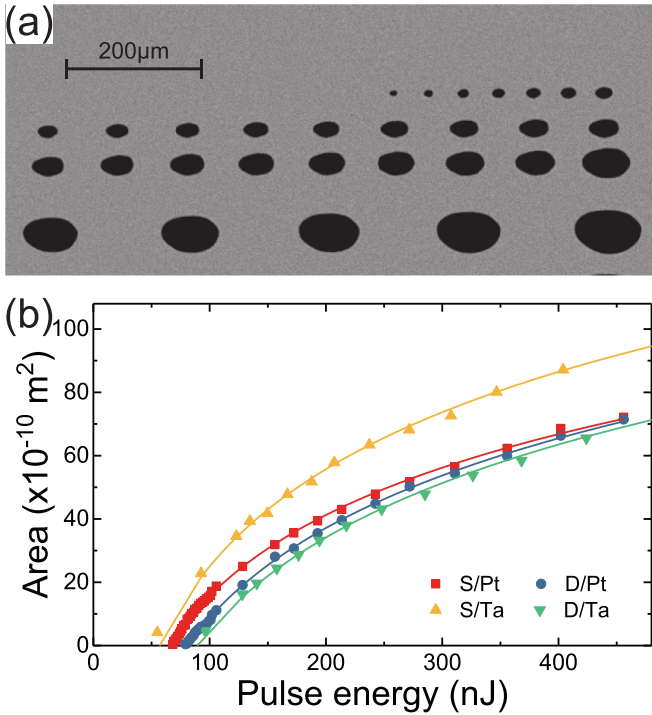


FIG. 3. Pulse-energy-dependent AOS measurement on Co/Gd stacks. (a) Kerr image of the switching experiments performed on S/Pt. An increasing domain area is observed upon increasing the pulse energy up to 450 nJ. (b) Domain size as a function of pulse energy for different structures. The minimum pulse energy to nucleate a domain (intercept of x axis) corresponds to the threshold energy P_0 .

skyrmionic bubbles, i.e., Néel-type domain walls with net chirality at zero fields when the DMI is strong enough. (ii) Moon shape patterns are produced by two successive, slightly displaced laser pulses, which converge to extremely thin, curved stripes if the displacement of the laser pulses is much smaller than the diameter of the laser spot, see Fig. 4(a). The latter one [type (ii)] will be discussed in the following part. We propose that the small domains display shape changes due to the laser's heating effect or the following creep processes. To describe the creeplike deformation of the narrow-stripe-domain, we successively address two parts: the sharp tip and the middle region.

For an ideal writing process, governed by an entirely local switching event with a well-defined threshold fluence, two moon-shaped domains are formed, touching in two singularities at opposite sides of the laser spot, where two domain walls cross. Such a structure is intrinsically unstable, as we verified by micromagnetic simulations below. At a time-scale of nanoseconds, the two touching domains will detach as illustrated in Fig. 4(a), ending up in two tapered domains with rounded ends. To further reduce their micromagnetic energy, these tapered ends will shrink as Fig. 4(b) illustrates. This shortening process is dominated by the reduction of domain wall energy to lower the total energy, where the domain wall energy density is defined as $\sigma = 4\sqrt{AK_{\text{eff}}} - \pi D$ (per unit area) [30,31]. In this way, not only A and K_{eff} but also the strength of DMI is related to the instability (shrinkage) of the

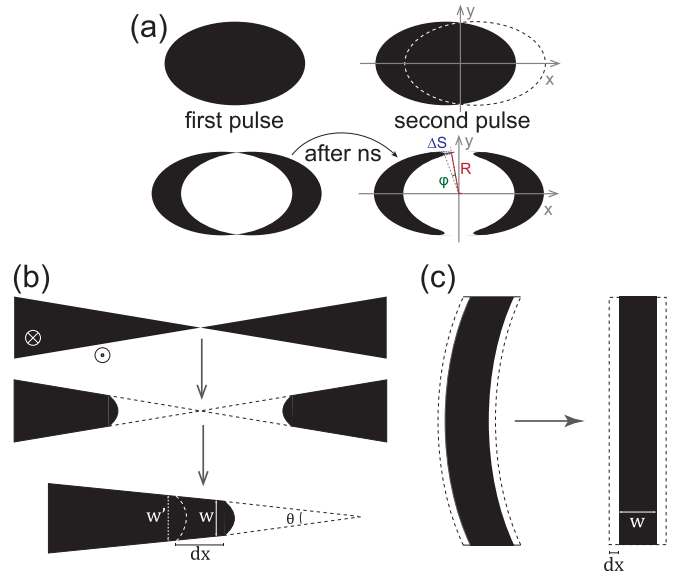


FIG. 4. (a) A schematic of moon-shape domain pairs writing by two toggle laser pulses. (b) Shortening process of domains on the sharp tips. (c) Widening process of domain strip.

domain at its tip end; the larger the DMI energy the larger its stability, and the slower the shrinkage.

To make an order of magnitude estimate of the effective field governing the shrinkage process, we approximate the tip end by a sharp triangle with a semicircular cap, where θ is the opening angle, w is the diameter, and t is the ferromagnetic layer thickness [see Fig. 4(b)]. In the limit of $\theta \rightarrow 0$, this structure can be considered as a stripe with fixed-width terminated by a semicircular cap. For this structure, the domain wall energy will reduce by $dE = 2\sigma t dx$ when the stripe contracts by dx . Neglecting the change in the dipolar field associated with this contraction, and comparing with the difference of Zeeman energy in an external field ($\Delta E = -\mathbf{m} \cdot \mathbf{B}$), the effective field corresponding to the reduction of DW energy can be written as $B_{\text{eff}}^{\text{DW}} = \frac{2\sigma t dx}{wtM_s dx} = \frac{2\sigma}{wM_s}$. Note that upon contraction, and assuming a small but finite value of θ , the value of w will increase, leading to a gradually slowing down of the shrinkage process.

However, this contraction will not continue indefinitely. When the width of the stripe w grows larger, dipolar energies, which strive to increase the stripe width, will increase. In order to obtain a simple estimate, we approximate the domain by a semi-infinite stripe with a straight cap. To avoid divergencies in the integral for dipolar energies, the domain wall width Δ should be assumed to be finite. According to the Biot-Savart's Law and the difference of energy, we derived an approximate equation for the effective field associated with the dipolar interaction: $B_{\text{eff}}^{\text{di}} = \frac{\mu_0 M_s t}{\pi w} \ln \left[\frac{(w - \Delta)^2}{\Delta^2} \right]$, where Δ is the width of DW (see Supplemental Material part IV [25]). To be noticed, $B_{\text{eff}}^{\text{di}}$ has the opposite sign as $B_{\text{eff}}^{\text{DW}}$. As a consequence, the total effective field of the shortening process can be expressed as

$$B_{\text{eff}}^{\text{sh}} = \frac{2(4\sqrt{AK_{\text{eff}}} - \pi D)}{wM_s} - \frac{\mu_0 M_s t}{\pi w} \ln \left[\frac{(w - \Delta)^2}{\Delta^2} \right]. \quad (2)$$

Note that, as a consequence, $B_{\text{eff}}^{\text{sh}}$ will fade out slowly with increasing w .

Finally, we note that near the center of the moon-shaped domain, it can be modeled as a stripe of width w with infinite length, corresponding to assuming $\theta \rightarrow 0$. In this limit, the broadening of the stripe at its center does not cost any domain wall energy, but dipolar interaction would result in a lower total energy with an increasing w . As a consequence, in this limit, there will always be a tendency to broaden. In practice, this process stops because the effective field becomes too small to lead to measurable creep, or the domain transforms into a shape with a less pronounced aspect ratio, in which the net driving force to reduce the DW energy may result in a net shrinkage everywhere, ultimately leading to a collapse of the complete domain. An expansion process driven by dipole interaction will be observed in the middle of the narrow domain, as seen in Fig. 4(c). Regarding the infinite length of the stripe domain (compared with its width), we can obtain the effective field

$$B_{\text{eff}}^{\text{ex}} = \frac{2\mu_0 M_{St}}{\pi w}. \quad (3)$$

Thus, it is found that the larger the domain width w , the smaller the driving field associated with the expansion. With a specific w and experimental M_{St} , $B_{\text{eff}}^{\text{ex}}$ of each structure can be quantitatively obtained. For our structures, with a width of at least 1 micrometer, and using typical parameters, this leads to effective fields of 0.4 mT or smaller. In order to make an estimate of the relevance of such an effective field for our samples, we measured the DW velocity as a function of perpendicular field (at zero in-plane field). We fitted the results for each sample using the relation between the creep velocity and the driving field $\ln(v) \sim (\mu_0 H_z)^{-\frac{1}{4}}$, and extrapolated the trends according to these fits (more details can be found in Supplemental Material part V [25]). Thus, our estimate of $B_{\text{eff}}^{\text{ex}}$ extrapolates to a maximum velocity less than $1 \mu\text{m}$ in several days for all samples, which means that in our case the expansion process is expected to be negligible. We note that this weak tendency of widening a domain at its center is related to the small magnetization of our films, as a consequence of the compensating Co and Gd moments, leading to small dipolar effects.

VII. SIMULATIONS OF DOMAINS SHAPE-CHANGE

We simulated the shape-change process of the moonlike domain pair by the micromagnetic package MUMAX3 [32] without applying any magnetic field and at $T = 0\text{K}$. A series of results can be seen in Fig. 5, where domain pairs with different step sizes (i.e., the displacement of the laser spot between firing the two successive pulses) share the same time scale marked at the right. The first line of Figs. 5(a)–5(c) corresponds to the relaxed state of each domain pair. We found that the spontaneous shortening process happens at a ns time scale after the creation of the domain. The shrinking velocity damps rapidly, in agreement with Eq. (2), while the smaller the step size the larger the shrinking velocity. Besides, there is not any clear expansion process during the short-term time scale for all of the step sizes in our simulation. Finally, we note the asymmetry in shrinkage at the top and bottom end of the

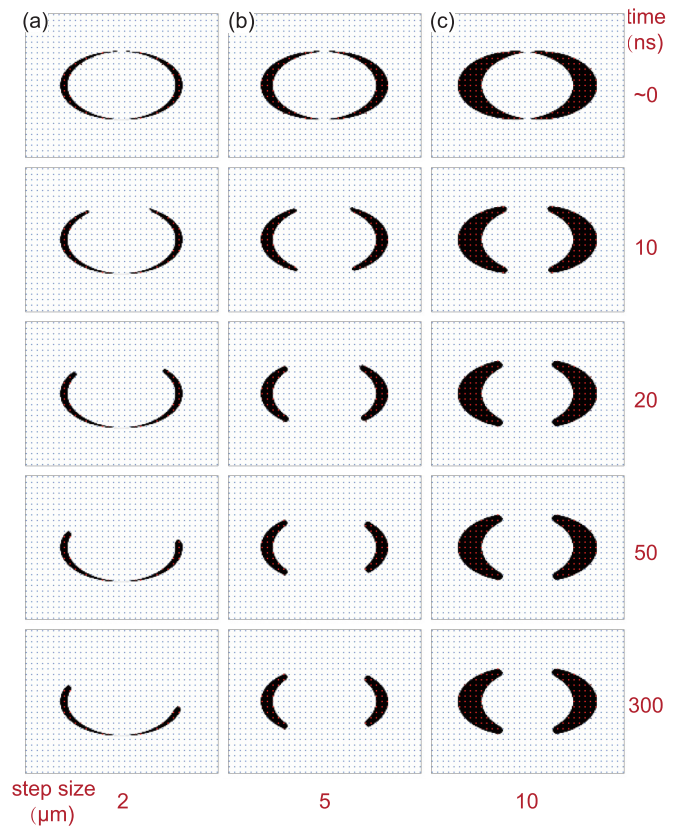


FIG. 5. Time-dependent shape-change of domains simulated by MUMAX3, with a step size of (a) $2 \mu\text{m}$, (b) $5 \mu\text{m}$, and (c) $10 \mu\text{m}$.

domain, particularly for the smallest step size [Fig. 5(a)]. This artefact is due to a combination of our finite mesh size and the pointlike anomaly in the initial state with crossing domain walls, but resolving it goes beyond the scope of this paper. More details about the simulations are given in Supplemental Material part VI [25].

VIII. EXPERIMENTAL OBSERVATIONS OF DOMAINS SHAPE-CHANGE

After understanding the main driving forces for the creeplike modifications of the AOS-written domains, the experimental results are discussed in this section. We generated moon-shaped domain-pairs by two consecutive laser pulses with a shift (step size) of 10, 5, 2, and $1 \mu\text{m}$. All samples were saturated by $\sim 56\text{mT}$ external field before the optical switching. Kerr images for switching results of different samples are shown in Fig. 6, sharing the scale bar shown in Fig. 6(d). All of the images were obtained within 5 min after AOS. Due to having its T_{comp} above room-temperature, **D/Pt** shows an inverse Kerr signal and correspondingly white domain areas, as compared to the black domains for the other three structures. It can be seen that the sharpest parts in the top and bottom ends of each domain-pair have eclipsed in a similar fashion as introduced in Figs. 4(a), 4(b), and 5. This demonstrates that an initial shortening process happened in the time interval between creating the domains and measuring the Kerr images. We also notice that the thinner domains (corresponding to largest θ and smallest w) produced with small step

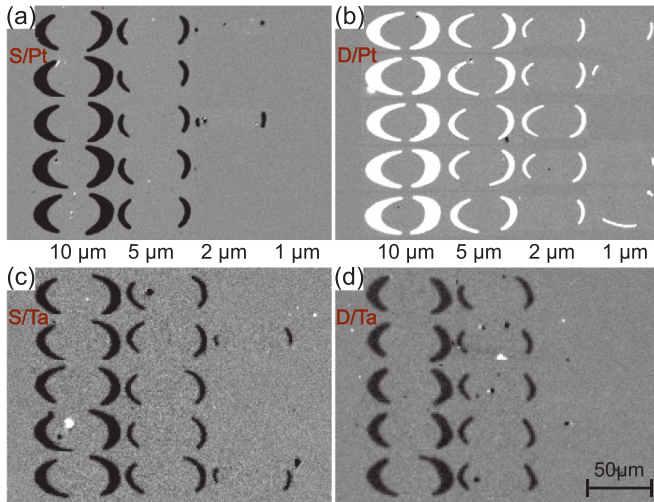


FIG. 6. The moon-shape domain pairs writing by two toggle laser pulses on the sample (a) S/Pt, (b) D/Pt, (c) S/Ta, and (d) D/Ta. Different step sizes result in different domains' width, while each column from left to right corresponding to step size 10, 5, 2, and 1 μm . Scale bar is shown in (d).

size suffer from stronger quenching processes, while more stable domains are produced with larger step sizes. We decreased the step sizes until the domains are unstable even at a time scale of minutes. For the **S/Pt**, **D/Pt**, **S/Ta**, and **D/Ta** structures, this led to a minimum step size of (roughly) 2, 1, 2, and 5 μm , respectively. According to Eq. (2), the effective driving field of the shortening process $B_{\text{eff}}^{\text{sh}}$ has a contribution that is proportional to the DW energy, which is negatively correlated to the DMI energy D . Comparing the domain images at 2- μm step size in Figs. 6(c) and 6(d), the sample with larger structural asymmetry (**S/Ta**) still shows some small domains, whereas all domains were completely quenched for the **D/Ta** sample. This behavior hints at a larger stability for domains in **S/Ta** structures, which is consistent with Eq. (2). Since **D/Pt** exhibit T_{comp} higher than room temperature, other complicated mechanisms might be involved in the domain's stability, so we refrain from a discussion of the group capped by Pt (**S/Pt** and **D/Pt**) here.

To describe the shape-change of domains more quantitatively and with specific emphasis on domain dynamics at a longer time scale, we analyzed the variance of the waist width and the opening angle, corresponding to the expansion and shrinkage, respectively. The definitions of the width and the opening angle (λ_l and λ_r) are given in Fig. 7(a). In passing we note that the observed difference between λ_l and λ_r can be explained by an asymmetry of the laser spot. For that reason, we averaged λ_l (left domain) and λ_r (right domain) of each domain pair with the same step size. Furthermore, we averaged width of domains within $\pm 5^\circ$ range around the x axis. The averaged λ , as well as the averaged width, as a function of time (after AOS) for each structure are shown in Figs. 7(b)–7(d).

We first focus on a possible widening effect. The dashed black lines in the top panels of Figs. 7(b)–7(d) represent the averaged width of the ideal shape (without expansion), which is determined by the corresponding step sizes. Taking the error

bars into account, the measured (averaged) width does not significantly deviate from the ideal values, i.e., there is not any observable expansion process in both the short-term and the long-term time scales after AOS.

Next, we address the shortening process, by inspecting the lower panels of Figs. 7(b)–7(d). Right after AOS, the initial value of λ (the average of λ_l and λ_r) should be 180° . The measured values are clearly smaller, corresponding to the initial shrinkage that we already qualitatively discussed before. Beyond this initial shrinkage that happens at a short time scale after AOS, the values of λ display a clear further reduction at a time scale of up to an hour. We fitted the trends of the averaged λ from 3 to 60 minutes by $\lambda = A - Bt$. The fitted parameter B is proportional to the shortening velocity at this longer time scale. Converted to domain wall velocities, values up to approximately 10^{-9} – 10^{-8} m/s are found. Detailed values are given in Supplemental Material part V [25]. The bottom panels in Figs. 7(b)–7(d) show that domains generated at smaller step size shorten faster than domains at larger step size, which is consistent with the simulation results shown in Fig. 5.

IX. DISCUSSION

Based on the above experimental results [Figs. 7(b)–7(d)] and physical model [Eq. (2)], we quantitatively compared the theoretical shortening velocity $v_{\text{th}}^{\text{sh}}$ with the experimental shortening velocity $v_{\text{ex}}^{\text{sh}}$, as well as the corresponding driving fields ($B_{\text{eff}}^{\text{sh}}$ and $\mu_0 H_{\text{ex}}^{\text{sh}}$). Results are shown in Figs. 7(e) and 7(f), respectively. **D/Pt** is omitted in this part due to the absence of reliable DMI measurements. First, we discuss how we derived the experimental values. We use the fitted parameter B to calculate $v_{\text{ex}}^{\text{sh}}$. In the limit of $\varphi \rightarrow 0$, $\theta \approx \tan\varphi$, and thus $v_{\text{ex}}^{\text{sh}} = \frac{\Delta S}{\Delta t} = \frac{R}{2} \frac{\Delta\lambda}{\Delta t}$, where R equals to the radius of a domain written by a single laser pulse (~ 25 μm in our case), ΔS stands for the shortening length within a period of time Δt , and $\frac{\Delta\lambda}{\Delta t}$ corresponds to the fitted value of B . The definition of ΔS , R , and φ can be found in Fig. 4(a). Extrapolating the measured field-induced DW velocities using the creep law, we also estimated the experimental driving field $\mu_0 H_{\text{ex}}^{\text{sh}}$. The error bar of the experimental data comes from the standard error of the fitted B . Next, we address how we derived the theoretical values. The driving field for shortening can be obtained from Eq. (2). $B_{\text{eff}}^{\text{sh}}$ can be calculated by adopting a value of exchange stiffness $A = 16$ pJ/m from the literature [28], using the saturation magnetization M_S and effective anisotropy K_{eff} from our experimental data (VSM data, assuming $t = 1.5$ or 3.0 nm), DW width $\Delta = \sqrt{A/K_{\text{eff}}}$, DMI energy D (as we introduced in the DMI section), and domain width w . To be noticed, we approximated the domain width w by the step size values to simplify the calculations, but verified that the error range on the domain width w does not significantly affect the order of $B_{\text{eff}}^{\text{sh}}$. Similarly, the theoretical shortening velocity $v_{\text{th}}^{\text{sh}}$ can be calculated by extrapolating our DW velocity data according to the creep law. Taking **S/Ta** as an example, we change the ferromagnetic layer thickness t from 1 to 4 nm (2–5 nm for D/X structure), recalculate M_S (per volume), K_{eff} (per volume), D , then obtained confidence intervals for $v_{\text{th}}^{\text{sh}}$ and $B_{\text{eff}}^{\text{sh}}$, shown as the light blue zones in Figs. 7(e) and 7(f). Detailed values of each parameter as well as the relation

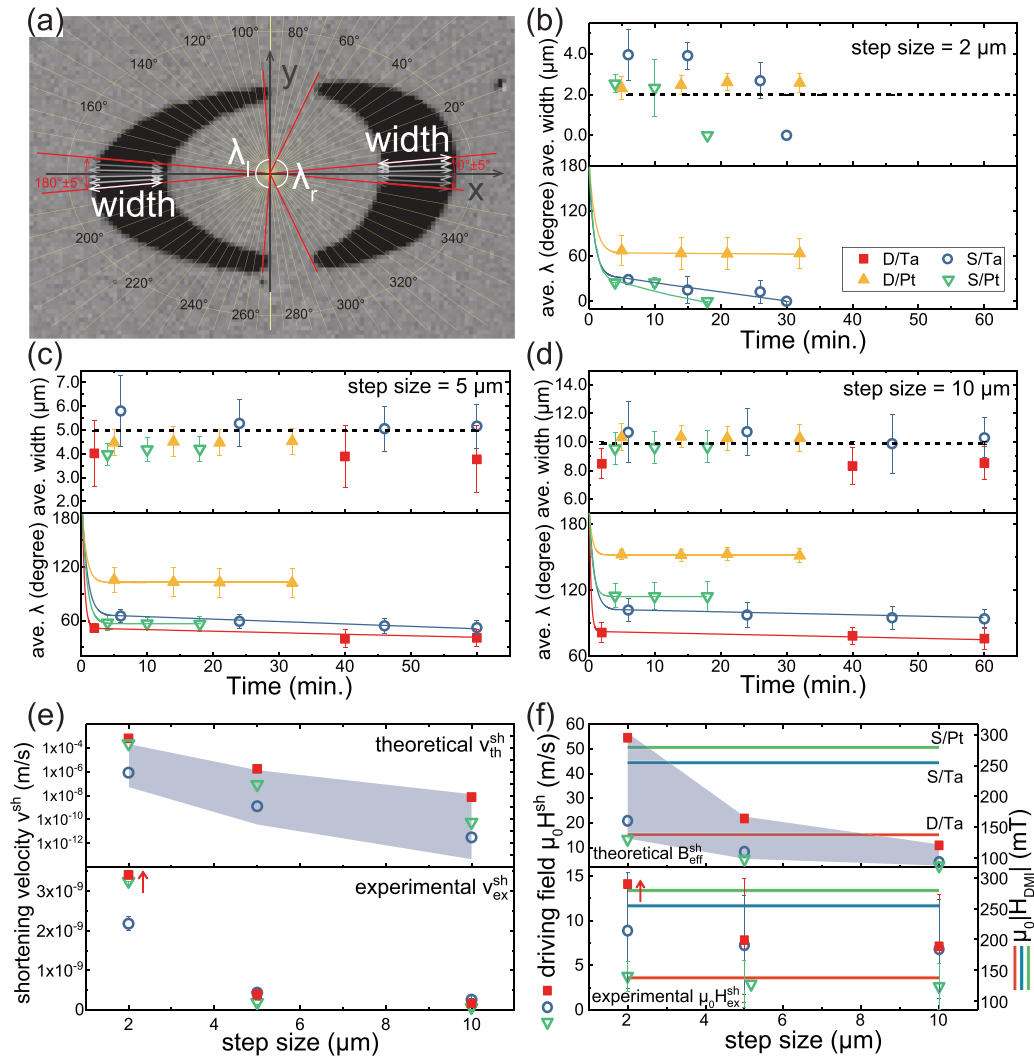


FIG. 7. (a) Kerr image of a domain-pair on **D/Ta** stacks, including the definition of width and λ in the later figures. (b)–(d) the time evolution of average width (top) and average λ (bottom) for domains written at 2, 5, and 10 μm step size during tens of minutes after AOS. The drawn lines are composed of the fitted linear trend at the timescale corresponding to the experimental data points, plus a guide to the eye at small time scales to stress the rapid initial shortening. Comparison of (e) shortening velocity and (f) driving field between experimental and theoretical data. Due to the uncertainty of the ferromagnetic layer thickness, we take **S/Ta** as an example, calculate confidence intervals for $v_{\text{th}}^{\text{sh}}$ and the corresponding $B_{\text{eff}}^{\text{sh}}$ shown in (e) and (f) as light blue zones. Note that at 2 μm step size all domains on **D/Ta** were quenched before the first Kerr image was taken, indicative for a large shortening velocity and driving field, as schematically indicated by the red arrow. (b)–(f) share a common legend shown in (b). The experimentally obtained DMI strength for **S/Pt**, **S/Ta**, and **D/Ta** is indicated in the two panels of (f) by lines in different colors.

between the creep velocity and the driving field are provided in Supplemental Material part V [25]. We also indicate the measured DMI field $\mu_0 |H_{\text{DMI}}|$ in Fig. 7(f) with red, blue, and green lines corresponding to **D/Ta**, **S/Ta**, and **S/Pt**, respectively. It can be seen that the structure with larger $\mu_0 |H_{\text{DMI}}|$ exhibits smaller $B_{\text{eff}}^{\text{sh}}$ and $\mu_0 H_{\text{ex}}^{\text{sh}}$, i.e., the existence of DMI is helpful for the stability of domains.

Comparing the experimental and theoretical estimates in Figs. 7(e) and 7(f), a reasonable agreement can be concluded. (i) Within order of magnitude the driving fields compare well; both the experiment and theoretical predictions yield fields of the order of 10 mT. Although due to the exponential behavior the theoretical velocities vary over many orders of magnitude, also there some overlap can be observed. (ii) We

found the same trend in shrinkage as a function of domain width. Both the theoretical and experimental results show that the shrinkage is more pronounced in narrower domains. (iii) As to the role of DMI, at 2- μm step size, a clear stabilizing effect of DMI is found in the Ta-capped set of samples. A lower DMI led to a quenching of all domains. For the data at larger step sizes, the experimental velocities and driving fields show a less systematic effect. The effect of DMI is certainly smaller than the theoretical values predict. As to the other discrepancies between theory and experiments, in particular the observation that the absolute values of $v_{\text{th}}^{\text{sh}}$ and $B_{\text{eff}}^{\text{sh}}$ are appreciably larger than $v_{\text{ex}}^{\text{sh}}$ and $\mu_0 H_{\text{ex}}^{\text{sh}}$, they can be attributed to several reasons. First, as described by our physical model on the shrinkage, under the limitation of $\theta \rightarrow 0$, the length

change of the semicircular cap Δw [from w to w' shown in Fig. 4(b)] can be neglected. In the case of a specific θ , the contribution of Δw would result in a smaller $\frac{2(4\sqrt{AK_{\text{eff}}-\pi D})}{wM_s}$ [positive term of Eq. (2)] and a smaller $B_{\text{eff}}^{\text{sh}}$. Second, with a specific θ , the dipole interaction would be larger, thus result in a larger $\frac{\mu_0 M_s t}{\pi w} \ln\left[\frac{(w-\Delta)^2}{\Delta^2}\right]$ [negative term of Eq. (2)] and also a smaller $B_{\text{eff}}^{\text{sh}}$. Third, the estimations of the DMI energy and the ferromagnetic layer thickness are quite rough. Finally, taking the light blue areas (confidence interval) in Figs. 7(e) and 7(f), as well as the error bars into account, we conclude that our model is in reasonable qualitative agreement with the experiments.

X. CONCLUSION

In conclusion, we explored the role of DMI on the dynamics of AOS-written domains in synthetic ferrimagnetic Pt/Co/Gd multilayers. Using stacks with single and double Co/Gd interfaces, which in the ideal case should correspond to asymmetric and symmetric structures, respectively, we distinguish between systems with large and small DMI. First, the compensation temperature was measured to confirm the synthetic-ferrimagnetic behavior of these stacks. Then the DMI strength was estimated by measuring asymmetric field-induced DW motion in the presence of an in-plane field. Next, we proposed a physical model for two types of shape-change in narrow domain stripes, i.e., a shortening and a widening process. Micromagnetic simulations and experimental observation on the optically written domains were also performed,

which qualitatively and quantitatively confirmed the shrinkage process and excluded the expansion process of domains. More specifically, a very fast shortening is observed, annihilating the unstable configuration of two crossing domain walls. Initial shortening occurs at a ns time scale, after which domain wall motion slows down rapidly. Only moon-shaped domains with an original width larger than 1–2 μm are not fully quenched within a time scale of several minutes, and the stabilizing role of DMI is resolved. Through the comparison between the theoretical and experimental results on the shrinkage of domains, we demonstrated the applicability of our model, which describes the role of DMI on the shortening process of optically switched domains. More specifically, we conclude that DMI as inherently built into the Pt/Co/Gd stacks, is helpful for stabilizing AOS-written small-size domain stripes. We notice that it is not trivial to scale down to submicron dimensions as would be required for large data densities, but our present study is expected to guide follow-up research aimed at reaching that goal.

ACKNOWLEDGMENTS

The authors thank the National Key R&D Program of China, Grant No. 2018YFB0407602, the National Natural Science Foundation of China (Grant No. 61571023), the International Collaboration Project B16001, the National Key Technology Program of China Grant No. 2017ZX01032101, the Program of Introducing Talents of Discipline to Universities in China (Grant No. B16001), the VR innovation platform from Qingdao Science and Technology Commission and the China Scholarship Council.

-
- [1] C. D. Stanciu, F. Hansteen, A. V. Kimel, A. Kirilyuk, A. Tsukamoto, A. Itoh, and T. Rasing, *Phys. Rev. Lett.* **99**, 047601 (2007).
- [2] A. R. Khorsand, M. Savoini, A. Kirilyuk, A. V. Kimel, A. Tsukamoto, A. Itoh, and T. Rasing, *Phys. Rev. Lett.* **108**, 127205 (2012).
- [3] S. Mangin, M. Gottwald, C. Lambert, D. Steil, V. Uhlir, L. Pang, M. Hehn, S. Alebrand, M. Cinchetti, G. Malinowski, Y. Fainman, M. Aeschlimann, and E. E. Fullerton, *Nat. Mater.* **13**, 286 (2014).
- [4] C.-H. Lambert, S. Mangin, B. S. D. C. S. Varaprasad, Y. K. Takahashi, M. Hehn, M. Cinchetti, G. Malinowski, K. Hono, Y. Fainman, M. Aeschlimann, and E. E. Fullerton, *Science* **345**, 1337 (2014).
- [5] B. Zhang, Y. Xu, W. Zhao, D. Zhu, X. Lin, M. Hehn, G. Malinowski, D. Ravelosona, and S. Mangin, *Phys. Rev. Appl.* **11**, 034001 (2019).
- [6] M. S. El Hadri, P. Pirro, C. H. Lambert, S. Petit-Watelot, Y. Quessab, M. Hehn, F. Montaigne, G. Malinowski, and S. Mangin, *Phys. Rev. B* **94**, 064412 (2016).
- [7] I. Radu, K. Vahaplar, C. Stamm, T. Kachel, N. Pontius, H. A. Du, T. A. Ostler, J. Barker, R. F. L. Evans, R. W. Chantrell, A. Tsukamoto, A. Itoh, A. Kirilyuk, and A. V. Kimel, *Nature (London)* **472**, 205 (2011).
- [8] J. H. Mentink, J. Hellsvik, D. V. Afanasiev, B. A. Ivanov, A. Kirilyuk, A. V. Kimel, O. Eriksson, M. I. Katsnelson, and T. Rasing, *Phys. Rev. Lett.* **108**, 057202 (2012).
- [9] A. J. Schellekens and B. Koopmans, *Phys. Rev. B* **87**, 020407(R) (2013).
- [10] S. Wienholdt, D. Hinzke, K. Carva, P. M. Oppeneer, and U. Nowak, *Phys. Rev. B* **88**, 020406(R) (2013).
- [11] R. F. L. Evans, T. A. Ostler, R. W. Chantrell, I. Radu, and T. Rasing, *Appl. Phys. Lett.* **104**, 082410 (2014).
- [12] S. Gerlach, L. Oroszlany, D. Hinzke, S. Sievering, S. Wienholdt, L. Szunyogh, and U. Nowak, *Phys. Rev. B* **95**, 224435 (2017).
- [13] M. L. M. Laliu, M. J. G. Peeters, S. R. R. Haenen, R. Lavrijsen, and B. Koopmans, *Phys. Rev. B* **96**, 220411(R) (2017).
- [14] Y. Xu, M. Hehn, W. Zhao, X. Lin, G. Malinowski, and S. Mangin, *Phys. Rev. B* **100**, 064424 (2019).
- [15] S. S. P. Parkin, M. Hayashi, and L. Thomas, *Science* **320**, 190 (2008).
- [16] M. L. M. Laliu, R. Lavrijsen, and B. Koopmans, *Nat. Commun.* **10**, 1 (2019).
- [17] B. Koopmans, G. Malinowski, F. D. Longa, D. Steiauf, M. Fähnle, T. Roth, M. Cinchetti, and M. Aeschlimann, *Nat. Mater.* **9**, 259 (2010).
- [18] M. Wietstruk, A. Melnikov, C. Stamm, T. Kachel, N. Pontius, M. Sultan, C. Gahl, M. Weinelt, H. A. Durr, and U. Boven-siepen, *Phys. Rev. Lett.* **106**, 127401 (2011).
- [19] M. Beens, M. L. M. Laliu, R. A. Duine, and B. Koopmans, *AIP Adv.* **9**, 125133 (2019).
- [20] M. Beens, M. L. M. Laliu, A. J. M. Deenen, R. A. Duine, and B. Koopmans, *Phys. Rev. B* **100**, 220409(R) (2019).

- [21] Y. Sun, Y. Ba, A. Chen, W. He, W. Wang, X. Zheng, L. Zou, Y. Zhang, Q. Yang, L. Yan, C. Feng, Q. Zhang, J. Cai, W. Wu, M. Liu, L. Gu, Z. Cheng, C. Nan, Z. Qiu, Y. Wu, J. Li, and Y. Zhao, *ACS Appl. Mater. Interfaces* **9**, 10855 (2017).
- [22] T. C. Hufnagel, S. Brennan, A. P. Payne, and B. M. Clemens, *J. Mater. Res.* **7**, 1976 (1992).
- [23] J. A. González, J. P. Andrés, M. A. Arranz, M. A. López de la Torre, and J. M. Riveiro, *J. Phys. Condens. Matter* **14**, 5061 (2002).
- [24] J. A. González, J. P. Andrés, M. A. López de la Torre, J. M. Riveiro, T. P. A. Hase, and B. K. Tanner, *J. Appl. Phys.* **93**, 7247 (2003).
- [25] See Supplemental Material at <http://link.aps.org/supplemental/10.1103/PhysRevB.102.104412> for (I) detailed analysis on the temperature dependence of the magnetic moment and extraction of T_{comp} in synthetic-ferrimagnetic structures; (II) fitting function for H_{DMI} ; (III) threshold fluence for structures with Si/SiO₂ and Si:B substrates; (IV) derivation of the effective field $B_{\text{eff}}^{\text{di}}$ corresponding to the dipolar interaction during the shortening process; (V) creep-region DW motions, experimental and theoretical velocities of each sample; and (VI) micromagnetic simulation of the domains shape-change, which includes Refs. [33,34].
- [26] D. M. F. Hartmann, R. A. Duine, M. J. Meijer, H. J. M. Swagten, and R. Lavrijsen, *Phys. Rev. B* **100**, 094417 (2019).
- [27] A. Cao, X. Zhang, B. Koopmans, S. Peng, Y. Zhang, Z. Wang, S. Yan, H. Yang, and W. Zhao, *Nanoscale* **10**, 12062 (2018).
- [28] M. Vanatka, J.-C. Rojas-Sanchez, J. Vogel, M. Bonfim, A. Thiaville, and S. Pizzini, *J. Phys. Condens. Matter* **27**, 326002 (2015).
- [29] J. M. Liu, *Opt. Lett.* **7**, 196 (1982).
- [30] M. Heide, G. Bihlmayer, and S. Blügel, *Phys. Rev. B* **78**, 140403 (2008).
- [31] S. Rohart and A. Thiaville, *Phys. Rev. B* **88**, 184422 (2013).
- [32] A. Vansteenkiste, J. Leliaert, M. Dvornik, M. Helsen, F. Garcia-sanchez, and B. Van Waeyenberge, *AIP Adv.* **4**, 107133 (2014).
- [33] K. Cherifi, C. Dufour, Ph. Bauer, G. Marchal, and Ph. Mangin, *Phys. Rev. B* **44**, 7733 (1991).
- [34] C. C. Katsidis and D. I. Siapkas, *Appl. Opt.* **41**, 3978 (2002).